HHS Public Access

Author manuscript

Biochemistry. Author manuscript; available in PMC 2016 February 17.

Published in final edited form as:

Biochemistry. 2015 February 17; 54(6): 1364–1370. doi:10.1021/bi5014722.

Effect of Interior Loop Length on the Thermal Stability and pK_a of i-Motif DNA

Samantha M. Reilly[†], **Rhianna K. Morgan**[‡], **Tracy A. Brooks**[‡], and **Randy M. Wadkins**[†,*]

[†]Department of Chemistry and Biochemistry, University of Mississippi, University, MS 38677

[‡] Department of BioMolecular Sciences, University of Mississippi, University, MS 38677

Abstract

The four-stranded i-motif (iM) conformation of cytosine-rich DNA has importance to a wide variety of biochemical systems that range from its use in nanomaterials to a potential role in oncogene regulation. An iM is stabilized by acidic pH that allows hemiprotonated cytidines to form a $C•C^+$ base pair. Fundamental studies to understand how the length of loops connecting the protonated $C•C^+$ pairs affect intramolecular iM physical properties are described in this report. We characterized both the thermal stability and the pK_a of intramolecular iMs with differing loop lengths, in both dilute solutions and in solutions containing molecular crowding agents. Our results showed that intramolecular iMs with longer central loops form at higher pH and temperature than iMs with longer outer loops. Our studies also showed that increases in thermal stability of iMs when molecular crowding agents are present are dependent on the loop that is lengthened. However, the increase in pK_a for iMs when molecular crowding agents are present is insensitive to loop length. Importantly, we also determined the proton activity of solutions containing high concentrations of molecular crowding agents to ascertain whether the increase in pK_a of an iM is due to alteration of this activity in buffered solutions. We determined that crowding agents alone increase the apparent pK_a of a number of small molecules as well as iMs, but that increases to iM pK_a were greater than that expected from a shift in proton activity.

Keywords

DNA Tetraplexes; i-DNA; G-quadruplexes

G4s and iMs are formed from guanine-rich and cytosine-rich sequences, respectively. Gellert et al.,[1] in 1962 showed that four guanine bases can hydrogen bond with each other to form G-tetrads. Later, Arnott et al.,[2] in 1974 showed that the array of G-tetrads stack to form G4s. The foundation of discovery of iMs was laid in 1963 when Langridge and Rich[3] proposed that cytosines in poly dC could hydrogen bond to form an ordered, hemiprotonated structure at low pH. However, it was only in 1993 that the four-stranded structure of iMs was determined (Figure 1).[4] Curiously, the preponderance of genomic DNA with potential G4/iM sequences is found in genes that regulate cell growth.[5] G4s and iMs are formed in

*Corresponding Author: rwadkins@olemiss.edu.

Supporting Information Available

This material is available free of charge via the Internet at http://pubs.acs.org.

G/C-rich DNA from promoters of genes involved in cell proliferation, including VEGF, kRAS, Bcl-2, pRb, PDGF-A, and MYC.[6, 7] Ever since these discoveries, the existence of G4s and iMs in living cells has remained a topic of great controversy. In 2013, Balasubramanian et al.,[8] published one of the first papers that confirmed G4s exist *in vivo*, which has been further supported by several additional reports on G4s *in vivo* in both DNA and RNA.[9-13] No similar studies for iMs have been performed, so their existence *in vivo* is still yet to be determined. Unlike G4s, iMs have not yet been considered widely as stable *in vivo* since the pH in the nucleus is believed to be not much different than cytosolic pH (~7.3)[14, 15] while the pK_a of a typical iM is < 7.0. However, recent studies from our lab and others[16-18] have shown that iMs indeed form at neutral pH when molecular crowding agents are present. Since cells and cell nuclei are crowded with biopolymers, this finding suggests iMs may be viable *in vivo* and deserve further study for comparison with the better-characterized G4 and Watson-Crick B-DNA structures.

In addition to their possible biological relevance, iMs are currently being used as a functional agent in biomaterials. Prior examples of iM use include biocompatible pH sensors and drug delivery vehicles. These applications take advantage of the iM's unique topology and proton dependence.[19-23] For example, Song et al.,[22] reported an iM-based gold nanomaterial that could deliver the anticancer drug doxorubicin specifically to human cervical adenocarcinoma cells cultured *in vitro*. The drug is intercalated into duplex DNA containing mismatching pairs that are attached to a gold nanomaterial. Once the nanomaterial reaches the hypoxic cancer cells, the microenvironment's low pH causes the DNA to fold into an iM, releasing the intercalated doxorubicin. The properties of these and other nanomaterials are directly linked to iM biophysical properties, such as their thermal stability and pK_a. Thus, better understanding the properties of iMs with varying characteristics will allow better control over the physical properties of iM-based nanomaterials.

Sequences that form iMs are usually derived from their corresponding G4 sequences that were located using Quadfinder[24] and/or Quadparser.[25] The default search in both Quadfinder and Quadparser is the sequence of $G_{3+}N_{1-7}G_{3+}N_{1-7}G_{3+}N_{1-7}G_{3+}$, where N stands for the loop residues and G for guanines. This default sequence has been based on multiple systematic studies that have shown that lengthening any loop of the G4 will decrease the thermal stability of the G4s, influence the type G4 formed, and increase the potassium dependence of G4 formation.[26-30] This search algorithm has also been used to find potential iMs on the opposite strand; however, the most stable G4 and iM formed from the same DNA duplex sequence of the c-MYC gene do not share the same loop lengths with the iM having much longer loops than its G4 counterpart.[31] Studies performed with DNA hairpins[32-35] show a decreased thermal stability with increasing loop length; however, hairpins can reach up to twenty bases in length and still be stable at physiological temperatures.[32, 34] The loop length effects in iMs have not been well characterized, and are the subject of this report.

To determine the optimal loop length to use in finding potential iMs, we examined the effect of loop length on an iM's structural stability. We determined the effects of loop length in dilute and molecular crowded buffers that more closely mimic intracellular conditions.[18, 36-40] We examined 16 different oligonucleotide sequences (oligos) differing in

both loop length and position (Table 1; Figure 1). Polyethylene glycol (PEG) was employed as the crowding agent since it is the most commonly used molecular crowding agents in the literature on both iMs and G4s.[18, 36-40] We used 40% PEG (w/w) to mimic cells since biomolecules can occupy 20 – 40% of cell volume.[17, 18, 41] Using circular dichroism (CD) spectroscopy and ultraviolet (UV) absorbance spectroscopy, we determined the thermal stability and pK_a of each oligo under dilute and molecular crowded conditions, where the size of PEGs used varied in average molecular weight from 300 to 3350. We did not go beyond 3350 since at least one previous report[17] states that PEGs with sizes above 4000 can bind to DNA secondary structures. Earlier studies reported that a high percentage (>30%) of other hydrophilic molecules, including PEG, shifted the apparent pH of buffered solutions.[42-46] To observe the effect of PEG on apparent pH, we analyzed five pH indicators and cytidine monophosphate to determine their pK_a values with and without PEG. Any increase in the pK_a of iMs greater than those arising from a change in proton activity (as observed with the indicators and cytidine monophosphate) can be attributed to PEG's crowding effect. By obtaining key details about iM sequence-dependent physical properties, our results may help guide the creation of novel iM-based nanomaterials with carefully tuned pH responses. Further, our results provide guidance for adjusting search algorithms to find potential iMs in genomic DNA sequences other than those that are complementary to G4 sequences.

Materials and Methods

Oligos

All DNA oligos (Table 1) were synthesized through standard solid-phase chemistry by Midland Certified Reagent Company, Inc. (Midland, TX, USA). All other reagents were purchased from Fisher Scientific (Waltham, MA, USA). The oligos were stored in 10 mM Tris, 1 mM EDTA buffer (pH 8.0) until use. The oligo sequence chosen (5'-CCC T CCC T CCC T CCC-3') is a non-physiological one chosen to minimize variables. The loop length substitutions were thymine repeats of varying length (1, 3, 5, 10, 15, and 20 thymines). Unless specifically stated otherwise, final solutions for all experiments were 4 μM DNA in 30 mM sodium cacodylate buffers of varying pH (5.4 to 8.0) either with or without 40% PEG of sizes as indicated in the text. Solutions were initially heated to ~ 80 °C for ten minutes and then cooled to room temperature to remove any multimeric duplex DNA present.

pK_a Determination

To determine the pK_a for iM folding (i.e., the pH at which 50% of the oligo is folded into the iM), CD spectra of DNA solutions at 20 °C were collected from 250-320 nm on an Olis DSM 20 Circular Dichroism (CD) instrument fitted with a peltier heat block (Olis, Inc. Bogart, GA, USA). An integration time as a function of high voltage was used. The CD signals observed at 298 nm were then plotted against pH, and then Equation 1 was applied to obtain pK_a and the cooperativity parameter.

$$Signal_{Total} = \frac{Signal_{Folded} - Signal_{Unfolded}}{1+10^{(Cooperativity*(pH-pKa))}} + Signal_{Unfolded} \quad \text{Equation 1}$$

Thermal Stability and Denaturation of iMs

Melting of iMs between 20 °C to 80 °C were determined by monitoring CD signals and/or UV absorbance at 1 °C intervals for all oligos (4 μM) at pH 5.4 with and without 40% PEG. After verifying iM melting on the CD, repeated thermal melts were also performed on a Cary 100 UV-Visible spectrometer (Agilent Technologies, Santa Clara, CA, USA) at 260 nm. The thermal denaturations were similar with either spectrometer. With an assumed two-state equilibrium model (as suggested by a isodichroic point at ~ 280 nm), we determined the melting temperature (T_m). All fractions were normalized such that the data ranged from 0 and 1 prior to fitting. The change in free energy at 37 °C ($\Delta G°_{37\,°C}$) was calculated by equation 2, where [N] and [U] are the concentrations of the iM and random coil forms of DNA, respectively, R is the gas constant, and T is physiological temperature (310 K).[47] In addition, to ensure the iMs formed were indeed intramolecular, a range of DNA concentrations (0.6 μM, 4 μM, and 20 μM) were analyzed for all oligos. All oligos were found to have the same T_m and $\Delta G°_{37°C}$ regardless of concentration, suggesting all oligos form an intramolecular iM structure.

$$K = \frac{[N]}{[U]} = e^{\frac{-\Delta G°}{RT}} \quad \text{Equation 2}$$

Relation of Measured pH to Proton Activity

The method of Gaboriaud[45] was used to compare apparent pH with proton activity in PEG solutions. The pH was measured by a high performance, micro glass-body, Tris-compatible, combination pH electrode with a platinum junction and 3 M potassium chloride filling solution (Model pHE-11, GeneMate, BioExpress, Kaysville, UT, USA). Five pH indicators were used: bromothymol blue; 4-nitrophenol; 3,4-dinitrophenol; methyl red; and phenol red. In addition, to directly compare to iMs, cytidine 5'-monophosphate was also used. The pH titration of each indicator was performed on a Cary 100 UV-Vis spectrometer over a wavelength range of 230– 800 nm. Each indicator was made with a 30 mM sodium cacodylate buffer with or without 40% PEG-300 or PEG-3350. The sample size was 3 mL, and 0.05 M NaOH was titrated into the sample at increments of 0.02 to 0.10 mL, dependent on the magnitude of the previous pH change. Once the spectra no longer changed with pH, the maximum absorbance values of the acidic form of each indicator, corrected for dilution factors, were plotted against their respective measured pH to determine the pK_a.

Results and Discussion

pK_a Determination

The pK_a of each oligo is given in Table 2 with representative graphs shown in Fig. 2. The trend in pK_a values observed for Mod2 is distinctly different from that of the other loop

modifications (Mod1 and Mod3). Mod2 oligos are able to maintain iM structure at higher pH and with longer loop lengths than the other modifications. For example, with ten bases in their respective loops, Mod2T10 has a pK_a of 6.62 while Mod1T10 and Mod3T10 have a pK_a of 6.13. The pK_a remains the same for the Mod2 oligos until more than ten bases have been added to the loop. These data suggest that the length of the central loop has less of an effect on the pK_a than the outer loops. The cooperativity parameter of all oligos, determined by fitting to Equation 1, did not change significantly (~ 3 for all iMs formed), indicating that extending the loops does not affect how the iM unfolds when shifting from an acidic to a more basic pH. These findings suggest that central loops (e.g., Mod2) shorter than fifteen bases and outer loops (e.g., Mod1 and Mod3) shorter than ten bases are potentially viable *in vivo*. This is remarkably different from the results for G4s where, in the absence of other structural features in the loop, loop lengths are usually limited to seven bases to be potentially viable *in vivo*.

Effects of PEG on Apparent pH

Given our[16], and others',[17, 18] data on the effect of PEG on iM pK_a, we investigated the difference between the pH determined by electrode measurement and the activity of protons in the PEG solutions as detected by small molecules. We examined five well-known pH indicators and cytidine monophosphate by monitoring the change in UV-Vis absorbance with change in pH in 30 mM sodium cacodylate buffer with and without 40% PEG-300. Changes in the pK_a observed for these indicators in PEG solutions were attributed to a change in proton activity, since molecular crowding should not significantly affect the pK_a of small molecules such as the indicators. As shown in Table 3, the observed pK_a of indicators consistently increased by 0.25 upon the addition of 40% PEG-300 to the buffer. We also tested the indicators with 40% PEG-3350 to see if the pK_a is affected by the size of PEG; no additional differences in pK_a were noted, suggesting the change in activity is linked to the percentage of PEG (w/w) in solution and not on PEG size.

Effects of PEG on iM pK_a

The pK_a of all oligos shows an increase upon adding PEG (Table 2); however, the increase in pK_a is not different between oligos of different loop lengths or positions. The lack of a difference in pK_a between these oligos suggests that the increase in pK_a caused by molecular crowding conditions is not dependent on loop length. Based on our oligos, the increase in pK_a is likely associated with the number of $C\text{-}C^+$ bonds, which all these iMs have in common. In addition, there was no significant change in the cooperativity of the iMs with addition of PEG-300 (~ 3 in both dilute and crowded buffers). The increase in pK_a with 40% PEG-300 ($+0.40 \pm 0.07$) is larger than the change observed with small molecules ($+0.25 \pm 0.03$; Table 3), suggesting that a change in proton activity alone does not account for the change of iM pK_a. We suggest that the additional increase in pK_a corresponds to the physical effects of molecular crowding, inhibiting the unfolding of the structure.

Next, we examined the effect of varying PEG size on pK_a with T1, Mod1T3, and Mod1T10. Mod1 oligos were chosen, as they are symmetric with Mod3 oligos, and they have distinct differences in thermal stability and pK_a among short (1 base), medium (3-5 bases), and long (10 bases) loops. The pK_a increased by ~ 0.4 when adding PEG-300 and by ~ 0.7 when

adding PEG-3350, showing that PEG size has a direct influence on the pK_a of iMs. This increase is constant across all loop lengths tested, further suggesting that the pK_a increase from crowding agents is not dependent on loop length. We conclude that the changes in pK_a we observed are due to molecular crowding alone since the change in proton activity (as determined from the indicators to be +0.25) is the same for both PEG-300 and PEG-3350 (Table 3). We also calculated the excluded volume for each PEG-DNA complex between 0 and 40% PEG (Table S1), using the approach of Spink and Chaires.[48] The T_m increase correlates well with excluded volume over the PEG size and loop lengths used, but the pK_a does not, suggesting that excluded volume alone cannot explain the effects that PEG and loop length have on the pK_a of an iM.

Thermal Denaturation of Folded i-Motifs

Thermal denaturations were performed on all folded oligos from Table 1. From the recorded spectra, the melting temperature (T_m) of each oligo was determined (Table 4; Fig. 3). All oligos were found to have the same T_m and $\Delta G°_{37°C}$ across a range of DNA concentrations (0.6 – 20 μM), suggesting all oligos form an intramolecular iM structure. The trends observed for the T_m's of Mod1 and Mod3 are similar as loop length increases; however, these T_m values are distinctly lower than Mod2 oligos of the same loop length. Mod2 oligos can incorporate loops much longer than Mod1 and Mod3. For example, the Mod2 oligos can have loops up to five bases long and not incur a change in the thermal stability. The trends in T_m found for these oligos suggest that longer central loops are more stable in iMs than in G4 oligos, displaying a trend more similar to those observed by DNA hairpins. In the Mod1 and Mod3 oligos, which behave similar to G4 oligos, the loop (Fig. 1 B & D) may be sterically hindered by the other loop, leading to destabilization. On the other hand, the central loop (Fig. 1 C) does not encounter such steric hindrance in our iM models, and would not in other iM systems unless 5` and/or 3` overhangs are present. All enthalpies of folding determined by Van't Hoff analysis of T_m data were approximately −5.0 kcal/mol per $C\text{-}C^+$ bond, which corresponds well with previously published melting enthalpies of iMs,[49] and suggests little or no bonding interactions arise due to the loops. When loops were lengthened, the entropy of folding decreased from −0.11 kcal/mol/K for a loop length of one to −0.20 kcal/mol/K for a loop length of twenty, regardless of loop location. As a better indicator of biological viability, we calculated standard state ΔG° of folding for each oligo at the physiological temperature of 37 °C ($\Delta G°_{37\,°C}$ in Table 4). Of all iMs examined, Mod2 iMs were most biologically viable, showing a negative $\Delta G°_{37\,°C}$ up to a loop length of twenty thymines (Mod2T20). The $\Delta G°_{37\,°C}$ for Mod2 oligos becomes less negative when the central loop is longer than five bases; however, the $\Delta G°_{37\,°C}$ values still suggest that long central loops could exist *in vivo*. In contrast, iMs formed by the Mod1 and Mod3 oligos become unfavorable at 37 °C when there are more than five thymines in the loop, suggesting long outer loops are not biologically viable.

Multiple studies[16-18] have shown that adding a molecular crowding agent increases the T_m of select iMs. We studied the effects of molecular crowding on the T_m and folding as a function of loop length (Table 4; Fig. 3). The melting temperature of all oligos increases in the presence of 40% PEG-300 as shown in Table 4; however, the magnitude of this increase in T_m is dependent on which loop is elongated. For example, in 40% PEG-300, when the

loops of the Mod1 or Mod3 oligos are elongated, the T_m increases by 6 – 8 °C, but if the loops of the Mod2 oligos are elongated, the T_m increases by 9 – 12 °C. These different trends in PEG solutions suggest that longer central loops are more stable in molecular crowded conditions than their outer loop counterparts. We again interpret this as the central loop not being sterically hindered by the other loops (Fig. 1 B-D), which allows for Mod2 oligos to fold into and retain the iM structure more readily than their Mod1 or Mod3 counterparts. The enthalpy of folding did not change significantly between the dilute buffer and 40% PEG-300 solutions. The $\Delta G°_{37\,°C}$ observed under crowding conditions shows a similar trend to the T_m values, with $\Delta G°_{37°C}$ of the Mod1 and Mod3 oligos ranging from −2 to +3 kcal/mol and $\Delta G°_{37°C}$ of the Mod2 oligos ranging from −4 to −1 kcal/mol.

We used the oligos T1, Mod1T3, and Mod1T10 to further examine the changes in melting temperature as the size of PEG increased (Table 5). The thermal stability of all oligos showed an increase in T_m in different PEG solutions until the PEG size was greater than a molecular weight of 600, which is in agreement with a previous study.[17] At PEG sizes above 600, the T_m remains constant. We surmise that the PEGs < 600 can readily fit into the space the iM needs to fold, preventing the iM from folding. However, the physical crowding of PEG outside of the space the iM folds still forces the iM together, thus the increase in T_m is a combination of these two effects. The PEGs > 600 cannot fit easily into the folding space, and thus does not hinder iM folding. In addition, unlike pK_a, the excluded volume (Table S1) correlated very well with the observed increase in T_m as PEG size and loop length increased. Consequently, the increase in the T_m comes purely from the physical crowding of the space around the iM by PEG.

Conclusion

In this paper, we demonstrated that iMs with five or more thymidines in the central loop can form at higher pH than those with loops near the termini of the iM-forming regions. We also established that the increase in pK_a of iMs (+0.40) when PEG is added is independent of loop length and position. From our indicator studies, we found that a portion of this increase in pK_a upon adding PEG is from a change in proton activity, but crowding appears to contribute additional iM stability at higher pH. Our studies also demonstrated that the thermal stabilities of the iMs with three or more bases in the central loop are much higher (~ 15 °C) than their outer loop counterparts when no 5` or 3` overhangs are present, displaying behavior more similar to DNA hairpins than G4s. When the iMs are in molecular crowded conditions, we found those with outer loops exhibit a T_m increase by 6 – 8 °C while those with central loops exhibit a T_m increase by 9 – 12 °C. Together, these trends show that not all loops can be considered equal in iM formation and indicate that iMs with long central loops have a higher melting temperature and pK_a than previously thought. Adjusting loop length may allow for better control of the physical properties of iM-based nanomaterials since we have demonstrated that small changes to the loop lengths greatly affect the pH and temperatures where iM formation occurs. In addition, we also have shown that iMs with long central loops are potentially viable *in vivo* at physiological temperature, even with loop lengths of 20 bases; however, performing similar studies with 5’ and 3’ overhangs present is needed before this can be readily assumed for iMs in genomic DNA. This finding suggests that the optimal search algorithm for locating potential iM-forming sequences in genomic

databases may need to be adjusted to be different from algorithms used for finding potential G4 sequences.

Supplementary Material

Refer to Web version on PubMed Central for supplementary material.

Acknowledgments

Funding Sources: The National Science Foundation under the Mississippi EPSCoR Grant No. NSF EPS-0903787 and the National Institute of Health's grant R15 CA173667-01A1 (Tracy Brooks, PI; Randy Wadkins, co-PI) supported this research.

Abbreviations and Textual Footnotes

DNA	Deoxyribonucleic Acid
RNA	Ribonucleic Acid
iM	i-Motif
C	Cytosine
G4	G-Quadruplex
G	Guanine
T	Thymine
VEGF	Vascular Endothelial Growth Factor
kRAS	Kirsten Rat Sarcoma Viral Oncogene Homolog
Bcl-2	B-Cell Lymphoma 2
pRb	Retinoblastoma Protein
PDGF-A	Platelet-derived Growth Factor Subunit A
MYC	V-Myc Avian Myelocytomatosis Viral Oncogene Homolog
PEG	Polyethylene Glycol
CD	Circular Dichroism

References

[1]. Gellert M, Lipsett MN, Davies DR. Helix formation by guanylic acid. Proc. Natl. Acad. Sci. USA. 1962; 48:2013–2018. [PubMed: 13947099]

[2]. Arnott S, Chandrasekaran R, Marttilla CM. Structures for polyinosinic acid and polyguanylic acid. Biochem J. 1974; 141:537–543. [PubMed: 4375981]

[3]. Langridge R, Rich A. Molecular structure of helical polycytidylic acid. Nature. 1963; 198:725–728. [PubMed: 13928676]

[4]. Gehring K, Leroy JL, Guéron M. A tetrameric DNA structure with protonated cytosine-cytosine base pairs. Nature. 1993; 363:561–565. [PubMed: 8389423]

[5]. Eddy J, Maizels N. Gene function correlates with potential for G4 DNA formation in the human genome. Nucleic Acids Res. 2006; 34:3887–3896. [PubMed: 16914419]

[6]. Brooks TA, Hurley LH. The role of supercoiling in transcriptional control of MYC and its importance in molecular therapeutics. Nature Rev Cancer. 2009; 9:849–861. [PubMed: 19907434]

[7]. Brooks TA, Kendrick S, Hurley L. Making sense of G-quadruplex and i-motif functions in oncogene promoters. FEBS J. 2010; 277:3459–3469. [PubMed: 20670278]

[8]. Biffi G, Tannahill D, McCafferty J, Balasubramanian S. Quantitative visualization of DNA G-quadruplex structures in human cells. Nat. Chem. 2013; 5:182–186. [PubMed: 23422559]

[9]. Biffi G, Di Antonio M, Tannahill D, Balasubramanian S. Visualization and selective chemical targeting of RNA G-quadruplex structures in the cytoplasm of human cells. Nat. Chem. 2014; 6:75–80. [PubMed: 24345950]

[10]. Biffi G, Tannahill D, Miller J, Howat WJ, Balasubramanian S. Elevated levels of G-quadruplex formation in human stomach and liver cancer tissues. PloS One. 2014; 9:e102711. [PubMed: 25033211]

[11]. Henderson A, Wu Y, Huang YC, Chavez EA, Platt J, Johnson FB, Brosh RM, Sen D, Lansdorp PM. Detection of G-quadruplex DNA in mammalian cells. Nucleic Acids Res. 2014; 42:860–869. [PubMed: 24163102]

[12]. Lam EYN, Beraldi D, Tannahill D, Balasubramanian S. G-quadruplex structures are stable and detectable in human genomic DNA. Nat. Commun. 2013; 4:1796. [PubMed: 23653208]

[13]. Yang TL, Lin L, Lou PJ, Chang TC, Young TH. Detection of cell carcinogenic transformation by a quadruplex DNA binding fluorescent probe. PloS One. 2014; 9:e86143. [PubMed: 24489694]

[14]. Bright GR, Fisher GW, Rogowska J, Taylor DL. Fluorescence ratio imaging microscopy: temporal and spatial measurements of cytoplasmic pH. J. Cell Bio. 1987; 104:1019–1033. [PubMed: 3558476]

[15]. Llopis J, McCaffery JM, Miyawaki A, Farquhar MG, Tsien RY. Measurement of cytosolic, mitochondrial, and Golgi pH in single living cells with green fluorescent proteins. Proc. Natl. Acad. Sci. USA. 1998; 95:6803–6808. [PubMed: 9618493]

[16]. Bhavsar-Jog YP, Van Dornshuld E, Brooks TA, Tschumper GS, Wadkins RM. Epigenetic modification, dehydration, and molecular crowding effects on the thermodynamics of i-motif structure formation from C-rich DNA. Biochemistry. 2014; 53:1586–1594. [PubMed: 24564458]

[17]. Cui J, Waltman P, Le VH, Lewis EA. The effect of molecular crowding on the stability of human c-MYC promoter sequence i-motif at neutral pH. Molecules. 2013; 18:12751–12767. [PubMed: 24132198]

[18]. Rajendran A, Nakano S, Sugimoto N. Molecular crowding of the cosolutes induces an intramolecular i-motif structure of triplet repeat DNA oligomers at neutral pH. Chem. Commun. 2010; 46:1299–1301.

[19]. Liu Z, Li Y, Tian C, Mao C. A smart DNA tetrahedron that isothermally assembles or dissociates in response to the solution pH value changes. Biomacromolecules. 2013; 14:1711–1714. [PubMed: 23647463]

[20]. Chen L, Di J, Cao C, Zhao Y, Ma Y, Luo J, Wen Y, Song W, Song Y, Jiang L. A pH-driven DNA nanoswitch for responsive controlled release. Chem. Commun. 2011; 47:2850–2852.

[21]. Modi S, Swetha MG, Goswami D, Gupta GD, Mayor S, Krishnan Y. A DNA nanomachine that maps spatial and temporal pH changes inside living cells. Nat. Nanotechnol. 2009; 4:325–330. [PubMed: 19421220]

[22]. Song L, Ho VHB, Chen C, Yang Z, Liu D, Chen R, Zhou D. Efficient, pH-triggered drug delivery using a pH-responsive DNA-conjugated gold nanoparticle. Adv. Healthc. Mater. 2013; 2:275–280. [PubMed: 23184521]

[23]. Wang C, Du Y, Wu Q, Xuan S, Zhou J, Song J, Shao F, Duan H. Stimuli-responsive plasmonic core–satellite assemblies: i-motif DNA linker enabled intracellular pH sensing. Chem. Commun. 2013; 49:5739–5741.

[24]. Scaria V, Hariharan M, Arora A, Maiti S. Quadfinder: server for identification and analysis of quadruplex-forming motifs in nucleotide sequences. Nucleic Acids Res. 2006; 34:683–685.

[25]. Huppert JL, Balasubramanian S. Prevalence of quadruplexes in the human genome. Nucleic Acids Res. 2005; 33:2908–2916. [PubMed: 15914667]

[26]. Guedin A, Gros J, Alberti P, Mergny J. How long is too long? Effect of loop size on G-quadruplex stability. Nucleic Acids Res. 2010; 38:7858–7868. [PubMed: 20660477]

[27]. Hazel P, Huppert J, Balasubramanian S, Neidle S. Loop-length dependent folding of G-quadruplexes. J. Am. Chem. Soc. 2004; 126:16405–16415. [PubMed: 15600342]

[28]. Rachwal PA, Findlow IS, Werner JM, Brown T, Fox KR. Intramolecular DNA quadruplexes with different arrangements of short and long loops. Nucleic Acids Res. 2007; 35:4214–4222. [PubMed: 17576685]

[29]. Risitano A, Fox KR. Influence of loop size on the stability of intramolecular DNA quadruplexes. Nucleic Acids Res. 2004; 32:2598–2606. [PubMed: 15141030]

[30]. Smargiasso N, Rosu F, Hsia W, Colson P, Baker ES, Bowers MT, De Pauw E, Gabelica V. G-quadruplex DNA assemblies: Loop length, cation identity, and multimer formation. J. Am. Chem. Soc. 2008; 130:10208–10216. [PubMed: 18627159]

[31]. Sun D, Hurley LH. The importance of negative superhelicity in inducing the formation of G-quadruplex and i-motif structures in the c-Myc promoter: implications for drug targeting and control of gene expression. J. Med. Chem. 2009; 52:2863–2874. [PubMed: 19385599]

[32]. Goddard NL, Bonnet G, Krichevsky O, Libchaber A. Sequence dependent rigidity of single stranded DNA. Phys. Rev. Lett. 2000; 85:2400–2403. [PubMed: 10978020]

[33]. Kuznetsov SV, Ren CC, Woodson SA, Ansari A. Loop dependence of the stability and dynamics of nucleic acid hairpins. Nucleic Acids Res. 2008; 36:1098–1112. [PubMed: 18096625]

[34]. Nayak RK, Van Orden A. Counterion and Polythymidine Loop-Length-Dependent Folding and Thermodynamic Stability of DNA Hairpins Reveal the Unusual Counterion-Dependent Stability of Tetraloop Hairpins. J. Phys. Chem. B. 2013; 117:13956–13966. [PubMed: 24144397]

[35]. Rentzeperis D, Alessi K, Marky LA. Thermodynamics of DNA hairpins: contribution of loop size to hairpin stability and ethidium binding. Nucleic Acids Res. 1993; 21:2683–2689. [PubMed: 8332464]

[36]. Kan ZY, Lin Y, Wang F, Zhuang XY, Zhao Y, Pang DW, Hao YH, Tan Z. G-quadruplex formation in human telomeric $(TTAGGG)_4$sequence with complementary strand in close vicinity under molecularly crowded condition. Nucleic Acids Res. 2007; 35:3646–3653. [PubMed: 17488850]

[37]. Kan ZY, Yao Y, Wang P, Li X. h. Hao Y. h. Tan Z. Molecular crowding induces telomere G - quadruplex formation under salt - deficient conditions and enhances its competition with duplex formation. Angew. Chem. Int. Ed. 2006; 45:1629–1632.

[38]. Miyoshi D, Matsumura S, Nakano S.-i. Sugimoto N. Duplex dissociation of telomere DNAs induced by molecular crowding. J. Am. Chem. Soc. 2004; 126:165–169. [PubMed: 14709080]

[39]. Zheng, K.-w.; Chen, Z.; Hao, Y.-h.; Tan, Z. Molecular crowding creates an essential environment for the formation of stable G-quadruplexes in long double-stranded DNA. Nucleic Acids Res. 2010; 38:327–338. [PubMed: 19858105]

[40]. Zhou J, Wei C, Jia G, Wang X, Feng Z, Li C. Human telomeric G-quadruplex formed from duplex under near physiological conditions: spectroscopic evidence and kinetics. Biochimie. 2009; 91:1104–1111. [PubMed: 19524012]

[41]. Miyoshi D, Nakao A, Sugimoto N. Molecular crowding regulates the structural switch of the DNA G-quadruplex. Biochemistry. 2002; 41:15017–15024. [PubMed: 12475251]

[42]. Travers F, Douzou P, Pederson T, Gunsalus IC. Ternary solvents to investigate proteins at zub-zero temperatures. Biochimie. 1975; 57:43–48. [PubMed: 238663]

[43]. Arakawa T, Timasheff SN. Mechanism of polyethylene glycol interaction with proteins. Biochemistry. 1985; 24:6756–6762. [PubMed: 4074726]

[44]. Chuy S, Bell LN. Buffer pH and pK_avalues as affected by added glycerol and sucrose. Food Res. Int. 2006; 39:342–348.

[45]. Gaboriaud R. Sur le comportement des acides non chargés dans les milieux eau-méthanol. C. R. Acad. Sci. 1966; 263:911–914.

[46]. Hui-Bon-Hoa G, Douzou P. Ionic strength and protonic activity of supercooled solutions used in experiments with enzyme systems. J. Biol. Chem. 1973; 248:4649–4654. [PubMed: 4718738]

[47]. Bruylants G, Wouters J, Michaux C. Differential scanning calorimetry in life science: Thermodynamics, stability, molecular recognition and application in drug design. Curr. Med. Chem. 2005; 12:2011–2020. [PubMed: 16101501]

[48]. Spink CH, Chaires JB. Effects of hydration, ion release, and exluded volume on the melting of triplex and duplex DNA. Biochemistry. 1999; 38:496–508. [PubMed: 9890933]

[49]. Kaushik M, Suehl N, Marky LA. Calorimetric unfolding of the bimolecular and i-motif complexes of the human telomere complementary strand, $d(C_3TA_2)_4$. Biophys. Chem. 2007; 126:154–164. [PubMed: 16822606]

[50]. Schwarzenbach RP, Stierli R, Folsom BR, Zeyer J. Compound properties relevant for assessing the environmental partitioning of nitrophenols. Environ. Sci. Technol. 1988; 22:83–92. [PubMed: 22195514]

[51]. Crofts A, Jackson J. Bromothymol blue and bromocresol purple as indicators of pH changes in chromatophores of Rhodospirillum rubrum. Eur. J. Biochem. 1969; 10:226–237. [PubMed: 5823098]

[52]. Espinosa S, Bosch E, Rosés M. Retention of ionizable compounds in high-performance liquid chromatography: 14. Acid–base pK values in acetonitrile–water mobile phases. J. Chromatogr. A. 2002; 964:55–66. [PubMed: 12198856]

[53]. Tobey SW. The acid dissociation constant of methyl red. A spectrophotometric measurement. J. Chem. Educ. 1958; 35:514.

[54]. Berthois Y, Katzenellenbogen JA, Katzenellenbogen BS. Phenol red in tissue culture media is a weak estrogen: implications concerning the study of estrogen-responsive cells in culture. Proc. Natl. Acad. Sci. USA. 1986; 83:2496–2500. [PubMed: 3458212]

[55]. Flogel M, Biltonen RL. The pH dependence of the thermodynamics of the interaction of 3'-cytidine monophosphate with ribonuclease A. Biochemistry. 1975; 14:2610–2615. [PubMed: 238566]

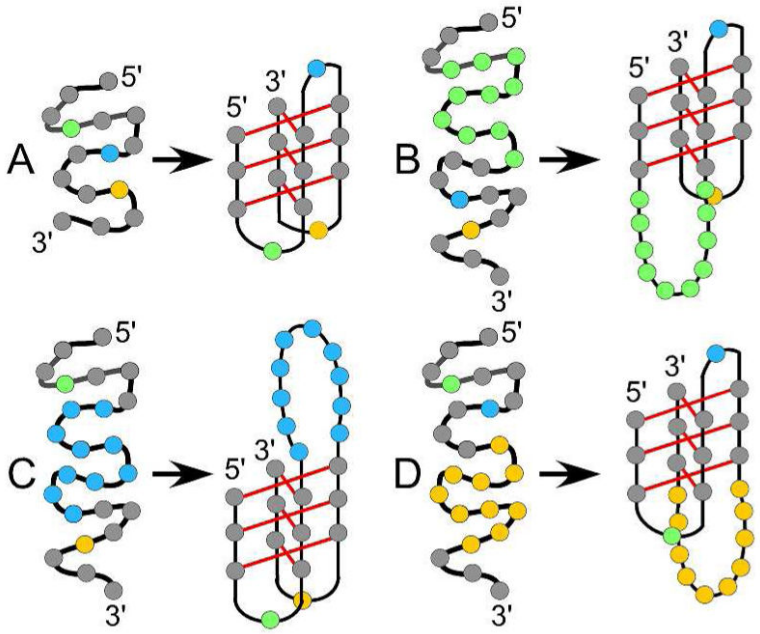

Figure 1.

Representative folding of a random coil into an iM for oligos differing by loop length and position: (A) a reference structure (T1) where all loops contain one thymine (colored spheres); (B) first (green; Mod1 oligos), (C) central (blue; Mod2 oligos), and (D) third (yellow; Mod3 oligos) loops have 3-20 thymines.

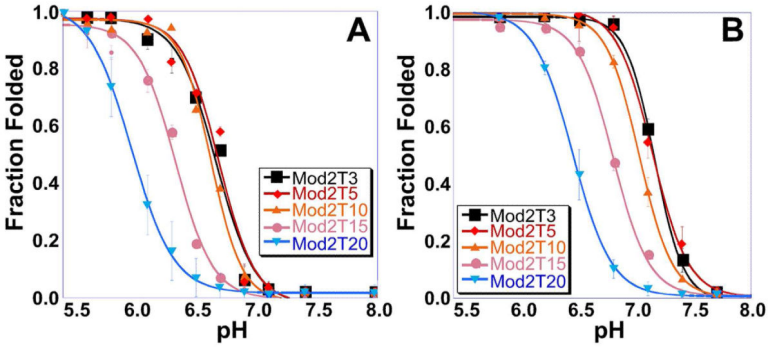

Figure 2.

Determination of pK_a of Mod2 oligos by monitoring the CD signal at 298 nm under (A) dilute buffer conditions and (B) molecular crowded conditions (40% PEG-300). The pK_a for these and the Mod1 and Mod3 oligos are recorded in Table 2.

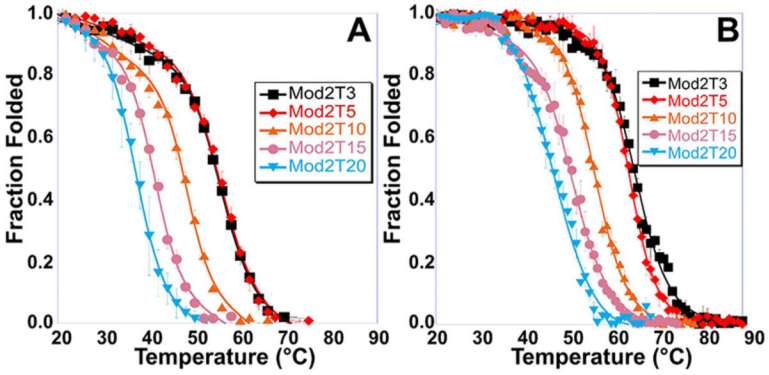

Figure 3.

Thermal denaturations of Mod2 oligos in (A) dilute buffer and (B) molecular crowded conditions (40% PEG-300). Both Mod1 and Mod3 showed similar trends. The T_m data obtained is recorded in Table 4.

Table 1

Oligos used and their respective sequences, where X is the location and number of the thymine repeats (3, 5, 10, 15, 20) in the loop modification

Name	5'-Sequence-3'
T1	CCC T CCC T CCC T CCC
Mod1TX	CCC **X** CCC T CCC T CCC
Mod2TX	CCC T CCC **X** CCC T CCC
Mod3TX	CCC T CCC T CCC **X** CCC

Table 2

The pK_a of all oligos in 30 mM sodium cacodylate ± 40% PEG-300. The ΔpK_a are also shown to emphasize the difference upon adding 40% PEG-300.

	pK_a No PEG	pK_a 40% PEG	ΔpK_a
T1	6.67 ± 0.01	7.03 ± 0.05	0.36
Mod1T3	6.66 ± 0.01	7.04 ± 0.05	0.38
Mod1T5	6.25 ± 0.04	6.71 ± 0.12	0.46
Mod1T10	6.14 ± 0.02	6.54 ± 0.05	0.40
Mod1T15	nd.*	nd.*	nd.*
Mod1T20	nd.*	nd.*	nd.*
Mod2T3	6.66 ± 0.03	7.16 ± 0.05	0.50
Mod2T5	6.68 ± 0.04	7.14 ± 0.05	0.46
Mod2T10	6.62 ± 0.02	6.98 ± 0.07	0.36
Mod2T15	6.33 ± 0.02	6.71 ± 0.06	0.38
Mod2T20	5.98 ± 0.05	6.48 ± 0.06	0.50
Mod3T3	6.70 ± 0.03	7.00 ± 0.06	0.30
Mod3T5	6.27 ± 0.02	6.63 ± 0.08	0.36
Mod3T10	6.12 ± 0.02	6.42 ± 0.05	0.30
Mod3T15	nd.*	nd.*	nd.*
Mod3T20	nd.*	nd.*	nd.*

*T_m of oligo ≤ 20 °C, thus pK_a not determined at 20 °C.

Table 3

pK_a determination for five pH indicators and cytidine monophosphate with two different sized PEGs at 40% (w/w) in 30 mM sodium cacodylate buffer

	pK_a 4-Nitro-phenol	**pK_a Bromo-thymol Blue**	**pK_a 3,4-Dinitro-phenol**	**pK_a Methyl Red**	**pK_a Phenol Red**	**pK_a Cytidine Mono-phosphate**
Lit. Value*	7.1	7.1	5.4	5.0	7.9	4.3
No PEG	7.10 ± 0.04	7.07 ± 0.03	5.31 ± 0.02	5.04 ± 0.04	7.98 ± 0.05	4.35 ± 0.06
PEG-300	7.33 ± 0.04	7.35 ± 0.04	5.52 ± 0.04	5.32 ± 0.03	8.27 ± 0.02	4.57 ± 0.04
PEG-3350	7.35 ± 0.06	7.36 ± 0.04	5.53 ± 0.02	5.28 ± 0.03	8.25 ± 0.02	4.61 ± 0.02
ΔpKa	0.24	0.28	0.22	0.26	0.28	0.24
ΔpKa (Avg.)	0.25 ± 0.03					

*References[50-55]

Table 4

The T_m and AG_{37} °C of all oligos in 30 mM sodium cacodylate ± 40% PEG-300. The ΔT_m and $\Delta\Delta G_{37\ °C}$ are also shown to emphasize the difference upon adding 40% PEG-300.

	T_m (°C) No PEG	T_m (°C) 40% PEG	ΔT_m (°C)	ΔG°37°C (kcal/mol) No PEG	$\Delta G°_{37°C}$ (kcal/mol) 40% PEG	$\Delta\Delta G°_{37°C}$ (kcal/mol)
T1	54.9 ± 0.4	58.5 ± 0.5	3.6	−2.2	−2.9	−0.7
Mod1T3	47.7 ± 0.4	53.3 ± 0.5	5.6	−0.9	−2.0	−1.1
Mod1T5	41.9 ± 0.3	48.8 ± 0.4	6.9	−0.6	−1.3	−0.7
Mod1T10	29.2 ± 0.5	37.5 ± 0.5	6.2	0.7	0.0	−0.7
Mod1T15	19.5 ± 0.4	25.8 ± 1.0	6.3	3.4	1.6	−1.9
Mod1T20	15.0 ± 0.5	21.0 ± 0.5	6.0	4.5	2.3	−2.2
Mod2T3	54.7 ± 0.3	66.7 ± 0.7	12.0	−2.3	−3.3	−1.1
Mod2T5	54.5 ± 0.6	64.0 ± 0.6	9.5	−2.7	−4.0	−1.3
Mod2T10	47.1 ± 0.2	55.8 ± 0.8	8.7	−1.6	−2.8	−1.2
Mod2T15	40.6 ± 0.1	49.8 ± 0.7	9.2	−0.7	−1.7	−0.9
Mod2T20	36.3 ± 0.6	46.2 ± 0.8	9.9	−0.6	−1.5	−0.9
Mod3T3	47.0 ± 0.4	55.4 ± 0.3	8.4	−0.8	−2.0	−1.3
Mod3T5	38.9 ± 0.6	45.5 ± 0.9	6.6	−0.3	−0.9	−0.7
Mod3T10	26.9 ± 0.1	34.3 ± 1.3	7.4	1.1	0.3	−0.8
Mod3T15	13.2 ± 0.3	21.2 ± 1.4	8.0	5.6	3.2	−2.4
Mod3T20	10.2 ± 0.2	17.9 ± 0.3	7.7	5.5	3.2	−2.2

Table 5

T_m of three iMs across different sized PEGs at 40% (w/w) in 30 mM sodium cacodylate at pH 5.4

	T_m (°C) T1	T_m (°C) Mod1T3	T_m (°C) Mod1T10
No PEG	54.9 ± 0.4	47.7 ± 0.4	29.2 ± 0.5
PEG-300	58.5 ± 0.5	53.3 ± 0.5	37.5 ± 0.5
PEG-600	59.1 ± 1.4	56.7 ± 0.9	44.0 ± 1.2
PEG-1500	65.3 ± 0.3	55.3 ± 1.0	47.4 ± 0.5
PEG-3350	65.0 ± 0.5	58.0 ± 0.5	48.8 ± 1.5